CHIRAL SYMMETRY BREAKING IN THE PAIRING MODEL OF QCD WITH THE COULOMB POTENTIAL

By A. Trzupek

Institute of Physics, Jagellonian University, Cracow*

(Received August 2, 1988)

Using the Bogoliubov-Valatin variational method we have analyzed the effect of the Coulomb potential on the chiral symmetry breaking in the pairing model of QCD. The renormalized gap equation for massless quarks interacting through the Lorentz vector potential $V(\vec{r}) \sim \sigma r - \frac{\alpha_s}{r}$ is solved numerically. An alternative derivation of the gap equation based on the Schwinger-Dyson equation is discussed. We also study the influence of the Coulomb term on the equation for the pion vertex function and on the pion properties. The chiral parameters and pion characteristics are also calculated in the baryonic background.

PACS numbers: 12.38.Lg

1. Introduction

Spontaneous breakdown of chiral symmetry is well established in hadron physics [1]. According to the standard argument, which was borrowed from the theory of superconductivity by Nambu and Jona-Lasinio [2], the dynamical chiral symmetry breaking is caused by the condensation of fermion pairs. The underlying mechanism responsible for the pair condensation is, however, still poorly understood in the framework of Quantum Chromodynamics [3]. The most promising tool, available at present to study this nonperturbative phenomenon, is the numerical simulation of Lattice Gauge Theory. Although, in principle, the lattice formulation allows us to solve Quantum Chromodynamics (QCD) completely, the inclusion of fermions on a lattice is still problematic and the technique is under development [4]. In continuum there are various attempts to find a good approximation to describe the spontaneous breakdown of chiral symmetry. One of them [5] analyzes a gap equation, written down in the Landau gauge in the linearized approximation. In this approach the ultraviolet behaviour of the dynamical quark mass can be studied. In the alternative method [6], which we are using in this article, the gap equation is considered in the Coulomb gauge within the instantaneous approximation. This approach is similar to the models used in

* Address: Instytut Fizyki UJ, Reymonta 4, 30-059 Kraków, Poland.

quarkonium spectroscopy and allows for using the phenomenological static potentials to describe the chiral symmetry breaking.

The model, originally proposed by Finger and Mandula, connects the Nambu and Jona-Lasinio mechanism with the basic properties of Quantum Chromodynamics. The vacuum of Quantum Chromodynamics is approximated by a coherent superposition of quark-antiquark pairs, and analyzed via the Bogoliubov-Valatin variational method. This leads us to the gap equation. The quark interaction is described by the chirally symmetric, normally ordered effective Hamiltonian derived from QCD Hamiltomian in the Coulomb gauge. The normal ordering in the second-quantization formalism is equivalent to the omission of the self-energy of quarks, which, for potential used there, is infinite. This approach, however, can not be applied to the confining potentials [7], because in this case the Casher instability criterion ($2p + V < 0$ [8]) can not be satisfied, as the potential $V(\vec{r}) = r^a$ is positive for all r's. Another argument, for changing the procedure is due to Adler and Davis [9], who noticed that the renormalization prescription (normal ordering) leads in general to the momentum *dependent* wave function renormalization constant. They also derived the correctly renormalized gap equation for general potential and solved it for the linear one. Simultaneously, the correct gap equation for confining potential was proposed in Ref. [7], where the authors pointed out that the instability criterion can be fulfilled when the quark self-energy, is taken into account (no normal ordering). This energy, which is negative, prevails over the kinetic and potential terms and leads to the chiral symmetry breaking. The gap equation for quadratic potential was also solved in Ref. [7]. Unfortunately, in both models resulting chiral parameters (such as the dynamical quark mass m^*, quark condensate $\langle \bar{u}u \rangle$, the pion decay constant f_π) were much smaller than the corresponding experimental numbers. One of the reasons to which this deviation was attributed [7, 9] is the lack of the Coulomb potential in the Hamiltonian. In this paper we analyze the full model containing the Coulomb and the linear potentials. We introduce the potential into the scheme in the way suggested in Ref. [9].

Another problem, which has recently attracted much interest, because of its importance for the heavy ion collision and for astrophysics, is the chiral symmetry restoration at finite temperature and baryonic number densities [10]. The present model has also been applied to the description of the phenomenon at finite temperature [11] and baryonic densities [12, 13]. The phase transition parameters (such as the critical Fermi momentum or baryonic density), which we have obtained in Ref. [13] for purely confining, linear potential $V(\vec{q}) \sim 1/q^4$, are again consistently smaller than expected from the experiment. In this paper we also investigate the recovery of chiral symmetry within the full model by solving the renormalized gap equation written in the baryonic background.

At the outset, in Section 2, we briefly review the main assumptions of the model and rederive the gap equation. This is achieved by introducing to the original Hamiltonian the counter-term, which removes the ultraviolet divergence caused by the Coulomb potential. An alternative derivation, which is based on the Schwinger-Dyson equation is also discussed. The influence of the Coulomb term on the equation for the pion vertex function and on the pion resulting properties is presented in Section 3. In Section 4 we analyze the effect of the baryonic background on the chiral parameters and pion characteristics in the presence of

the Coulomb potential. In Section 5 we solve numerically the gap equation and Bethe-Salpeter equation for the pion, with the aid of the overrelaxed Gauss-Seidel algorithm, and compute the chiral parameters. Section 6 contains discussion of the results and conclusions. In the Appendix A we detail the Green function approach to the gap equation. In the Appendix B we present a brief derivation of the homogeneous Bethe-Salpeter equation from the general inhomogeneous one. The expression for the pion charge radius is given in the Appendix C.

2. *Review of the model — the gap equation*

Let us discuss the two equivalent derivations of the gap equation. In the first one [6], this equation results from the minimalization condition imposed on the energy of the trial Bogoliubov-Valatin state. This method displays close relation between our model and BCS theory. The second approach [9], via the Green function method, allows us to derive correctly renormalized gap equation starting form the Schwinger-Dyson equation for the quark selfenergy $\Sigma(\vec{k})$.

1.1. The Bogoliubov-Valatin transformation

The effective Hamiltonian, introduced first in Ref. [6], for massless quark fields interacting through the fourth component of instantaneous Lorentz vector potential, reads

$$H = \sum_{\vec{x}} \psi^{\dagger}(\vec{x})\,(-\vec{\alpha}\cdot\vec{\nabla})\psi(\vec{x}) + \tfrac{1}{2}\sum_{\vec{x},\vec{y},\beta} \tilde{V}(\vec{x}-\vec{y})\left(\psi^{\dagger}(\vec{x})\frac{\lambda^{\beta}}{2}\psi(\vec{x})\right)\left(\psi^{\dagger}(\vec{y})\frac{\lambda^{\beta}}{2}\psi(\vec{y})\right)$$
$$+(Z-1)\sum_{\vec{x}} \psi^{\dagger}(\vec{x})\,(-\vec{\alpha}\cdot\vec{\nabla})\psi(\vec{x}). \tag{2.1}$$

The discretization is introduced in order to regularize the singularities, which emerge in further steps. Final expressions are derived in the continuum limit. $\vec{\alpha}$, λ^{β}, $\beta = 1,\ldots 8$ are Dirac and Gell-Mann matrices correspondingly, $\psi(\vec{x})$ is the coloured, single flavour, massless quark field. The generalization to the case of two flavours is straightforward. We expand this field in the massless, free spinor basis v^0, u^0

$$\psi_{\alpha}(\vec{x}) = \frac{1}{n^{3/2}}\sum_{\vec{k},s}\left[u^0_{s\alpha}(\vec{k})b^0_{s\alpha}(\vec{k}) + v^0_{s\alpha}(\vec{k})d^{0\dagger}_{s\alpha}(-\vec{k})\right]e^{i\vec{k}\cdot\vec{x}}, \tag{2.2}$$

where $b^0_{s\alpha}(\vec{k})$ and $d^0_{s\alpha}(\vec{k})$ denote the annihilation operators for a massless quark and antiquark with colour index α, helicity s and momentum $\vec{k}$. The potential $\tilde{V}(\vec{x})$ is equal to[1]

$$\tilde{V}(\vec{x}) = -\left(\sigma r - \frac{\alpha_s}{r}\right), \tag{2.3}$$

[1] The minus sign ensures attractive force between the $\bar{q}q$ in a colour-singlet state.

where $r = |\vec{x}|$. The last expression in Hamiltonian (2.1) is a counter-term, necessary to obtain finite results [7].

Analogously to the BCS description of the superconductivity, the vacuum in the model is approximated by a coherent superposition of the colour singlet $q\bar{q}$ pairs

$$|\Omega\rangle = \frac{1}{N}\prod_{\vec{k},s,\alpha}(1 - s\tau\beta(k)b^{0\dagger}_{s\alpha}(\vec{k})d^{0\dagger}_{s\alpha}(-\vec{k}))\,|0\rangle, \tag{2.4}$$

where $N = \prod_{\vec{k},s,a}\sqrt{1+\beta^2(k)}$ denotes the normalization factor, and τ is the volume element in the momentum space. This non-perturbative state $|\Omega\rangle$ is chirally asymmetric unless $\beta = 0$ — in this case $|\Omega\rangle$ reduces to the chirally symmetric, perturbative vacuum $|0\rangle$. The momentum space wave function of a quark-antiquark pair $\beta(\vec{k})$ is determined by the gap equation

$$\frac{\delta\langle\Omega|H|\Omega\rangle}{\delta\beta(\vec{k})} = 0. \tag{2.5}$$

Similarly to the theory of superconductivity, it is convenient to calculate the matrix element $\mathscr{E} = \langle\Omega|H|\Omega\rangle$ with the aid of the Bogoliubov-Valatin (B-V) transformation. To this end, one introduces the linear combinations (for each colour)

$$\begin{aligned}
b_s(\vec{k}) &= \cos\frac{\phi(k)}{2}\,b^0_s(\vec{k}) + s\sin\frac{\phi(k)}{2}\,d^{0\dagger}_s(-\vec{k}),\\
sd_s(\vec{k}) &= -\sin\frac{\phi(k)}{2}\,b^{0\dagger}_s(\vec{k}) + s\cos\frac{\phi(k)}{2}\,d^0_s(-\vec{k}),\\
u_s(\vec{k}) &= \cos\frac{\phi(k)}{2}\,u^0_s(\vec{k}) + s\sin\frac{\phi(k)}{2}\,v^0_s(\vec{k}),\\
v_s(\vec{k}) &= \cos\frac{\phi(k)}{2}\,v^0_s(\vec{k}) - s\sin\frac{\phi(k)}{2}\,u^0_s(\vec{k}).
\end{aligned} \tag{2.6}$$

One can show, that the state $|\Omega\rangle$, given by (2.4), constitutes the vacuum for the new creation and annihilation operators b, d, $b^\dagger$, $d^\dagger$, provided that

$$\sin\frac{\phi(k)}{2} = \frac{\beta(k)}{\sqrt{1+\beta^2(k)}} \quad \text{and} \quad \cos\frac{\phi(k)}{2} = \frac{1}{\sqrt{1+\beta^2(k)}}. \tag{2.7}$$

It follows by direct computation that the quasiparticle operators satisfy the Fermi-Dirac statistic. The B-V transformation consists of expressing the quark field and the Hamiltonian in terms of the new spinor basis u, v

$$\psi_\alpha(\vec{x}) = \frac{1}{n^{3/2}}\sum_{\vec{k},s}[u_{s\alpha}(\vec{k})b_{s\alpha}(\vec{k}) + v_{s\alpha}(\vec{k})d^\dagger_{s\alpha}(-\vec{k})]e^{i\vec{k}\cdot\vec{x}}. \tag{2.8}$$

Now, the matrix element can be easily calculated with the aid of the Wick's theorem. It allows us to rewrite the Hamiltonian in the following form[2]

$$H = \mathscr{E} + :H_2: + :H_4:, \tag{2.9}$$

with

$$\mathscr{E} = 3Z \sum_{\vec{k}} \mathrm{Tr}\,[(\vec{\alpha}\cdot\vec{k})\Lambda_-(\vec{k})] + \frac{4}{(an)^3} \sum_{\vec{k},\vec{p}} \tfrac{1}{2} V(\vec{k}-\vec{p})\,\mathrm{Tr}\,[\Lambda_+(\vec{k})\Lambda_-(\vec{p})],$$

$$H_2 = \tfrac{2}{3}\frac{1}{n^3} \sum_{\vec{x},\vec{y},\vec{k}} \tilde{V}(\vec{x}-\vec{y})\,[\psi^\dagger(\vec{x})\,(\Lambda_+(\vec{k})-\Lambda_-(\vec{k}))\psi(\vec{y})]e^{i\vec{k}\cdot(\vec{x}-\vec{y})}$$

$$+ Z \sum_{\vec{x}} \psi^\dagger(\vec{x})\,(-i\vec{\alpha}\cdot\vec{\nabla})\psi(\vec{x}),$$

$$H_4 = \sum_{\vec{x},\vec{y},\beta} \tfrac{1}{2}\tilde{V}(\vec{x}-\vec{y}) \left(\psi^\dagger(\vec{x})\frac{\lambda^\beta}{2}\psi(\vec{x})\right)\left(\psi^\dagger(\vec{y})\frac{\lambda^\beta}{2}\psi(\vec{y})\right). \tag{2.10}$$

$\Lambda_\pm(\vec{k})$ denote the projection operators (contractions) and are defined ($\hat{k} = \vec{k}/|\vec{k}|$) by

$$\overbrace{\psi_\alpha(\vec{x})\psi^\dagger_\beta(\vec{y})} = \sum_{\vec{k}} [\Lambda_+(\vec{k})]_{\alpha\beta} e^{i\vec{k}\cdot(\vec{x}-\vec{y})},$$

$$\overbrace{\psi^\dagger_\alpha(\vec{x})\psi_\beta(\vec{y})} = \sum_{\vec{k}} [\Lambda_-(\vec{k})]_{\alpha\beta} e^{-i\vec{k}\cdot(\vec{x}-\vec{y})},$$

to give

$$\Lambda_\pm(\vec{k}) = \tfrac{1}{2}(1 \pm \beta \sin\phi(k) \pm \vec{\alpha}\cdot\hat{k}\cos\phi(k)). \tag{2.11}$$

$V(\vec{k})$ is the Fourier transform of the potential

$$V(\vec{k}) = a^3 \sum_{\vec{x}} \tilde{V}(\vec{x}) e^{i\vec{k}\cdot\vec{x}} = V_L(\vec{k}) + V_c(\vec{k}), \tag{2.12}$$

with [7]

$$V_L(\vec{k}) = \frac{8\pi\sigma}{(\vec{k})^4} \quad \text{and} \quad V_c(\vec{k}) = \frac{4\pi\alpha_s}{(\vec{k})^2}. \tag{2.13}$$

Inserting Eqs. (2.9)–(2.11) into Eq. (2.5) gives the nonlinear integral gap equation

$$k\sin\phi(k) = (1-Z)k\sin\phi(k)$$

$$+ \tfrac{2}{3}\int \frac{d^3p}{(2\pi)^3} V(\vec{p}-\vec{k})\,(\sin\phi(p)\cos\phi(k) - \hat{k}\hat{p}\sin\phi(k)\cos\phi(p)), \tag{2.14}$$

[2] The normal ordering in this model was studied in papers [7, 16].

where in the continuum limit

$$a^3 \sum_{\vec{x}} \to \int d^3x, \quad \frac{1}{(an)^3} \sum_{\vec{p}} \to \int \frac{d^3p}{(2\pi)^3}. \tag{2.15}$$

However, the Coulomb potential in Eq. (2.13) introduces logarithmic divergences unless the appropriate renormalization is performed. The ultraviolet singularity can be eliminated with the aid of the momentum independent renormalization constant

$$Z-1 = -\frac{1}{k}\frac{2}{3}\int \frac{d^3p}{(2\pi)^3} V_c(\vec{p}-\vec{k})\hat{k}\hat{p}. \tag{2.16}$$

Performing the integrations over angles, after inserting the Eq. (2.16) into (2.14), we arrive at the ultraviolet finite, one-dimensional equation

$$k \sin \phi(k) \tag{2.17}$$

$$= \frac{2}{3\pi}\int_0^\infty dp(I_2^L(k, p) \sin \phi(p) \cos \phi(k) - I_1^L(k, p) \sin \phi(k) \cos \phi(p))$$

$$+ \frac{2}{3\pi}\int_0^\infty dp\left(I_2^c(k, p) \sin \phi(p) \cos \phi(k) + 2I_1^c(k, p) \sin \phi(k) \sin^2 \frac{\phi(p)}{2}\right),$$

where

$$I_2^L(k, p) = \frac{p^2}{4\pi}\int_{-1}^{1} d(\hat{k}\hat{p}) V_L(\vec{k}-\vec{p}) = \frac{4\sigma p^2}{(k^2-p^2)^2},$$

$$I_1^L(k, p) = \frac{p^2}{4\pi}\int_{-1}^{1} d(\hat{k}\hat{p})\hat{k}\hat{p} V_L(\vec{k}-\vec{p}) = \frac{k^2+p^2}{2kp} I_2^L(k, p) - \frac{\sigma}{k^2}\log\left|\frac{p+k}{p-k}\right|,$$

$$I_2^c(k, p) = \frac{p^2}{4\pi}\int_{-1}^{1} d(\hat{k}\hat{p}) V_c(\vec{k}-\vec{p}) = -\frac{\alpha_s p}{k}\log\left|\frac{p-k}{p+k}\right|,$$

$$I_1^c(k, p) = \frac{p^2}{4\pi}\int_{-1}^{1} d(\hat{k}\hat{p})\hat{k}\hat{p} V_C(\vec{k}-\vec{p}) = \frac{k^2+p^2}{2kp} I_2^c(k, p) - \frac{\alpha_s p}{k}. \tag{2.18}$$

The infrared ($p = k$) finiteness of the Coulomb part in Eq. (2.17) is obvious. It is readily seen from the Eq. (2.18), that the Coulomb contribution is integrable. On the other hand, the infrared finiteness of the linear potential term was discussed in Ref. [7]. It is ensured by

using the colourless trial states. As a consequence one can add an arbitrary constant to the potential without changing the results. The contribution from constant potential vanishes between colour singlets, since it is proportional to the Casimir operator of the colour symmetry group.

2.2. The Green function approach

Let us now discuss an alternative derivation of the gap equation, namely from the renormalized Schwinger-Dyson equation for the quark propagator [6]. This approach allows us to see more clearly the approximations which lead to the gap equation. To this end, we make the nonrelativistic ansatz for the quark self-energy

$$\Sigma(\vec{k}) = |\vec{k}|A(|\vec{k}|)+\vec{k}\cdot\vec{\gamma}B(|\vec{k}|). \tag{2.19}$$

Scalar functions $A(|\vec{k}|)$, $B(|\vec{k}|)$ are determined by the equation (see Appendix A)

$$\Sigma(\vec{k}) = (Z-1)\vec{k}\cdot\vec{\gamma}+\frac{1}{6\pi^3}\int d^3pV(\vec{k}-\vec{p})\gamma^0S^{(3)}(\vec{p})\gamma^0, \tag{2.20}$$

where $S^{(3)}(\vec{p})$ is the quark propagator ($S^{(4)}$) integrated over p^0 ($p = |\vec{p}|$)

$$S^{(3)}(\vec{p}) = \int\frac{dp^0}{2\pi}\frac{i}{p^0\gamma^0-\vec{p}\vec{\gamma}-\Sigma(\vec{p})} = \frac{pA(p)-(B(p)+1)\vec{\gamma}\vec{p}}{2\omega(p)},$$

with

$$\omega(p) = p\sqrt{A^2(p)+(B(p)+1)^2}. \tag{2.21}$$

From the definition of the equal time quark propagator

$$\int\frac{d^4p}{(2\pi)^4}S^{(4)}_{\alpha\beta}(\vec{p},p^0)e^{i\vec{p}\cdot(\vec{x}-\vec{y})} = \langle\Omega|\tfrac{1}{2}[\psi_\alpha(\vec{x}),\bar{\psi}_\beta(\vec{y})]|\Omega\rangle \tag{2.22a}$$

and with the aid of Eq. (2.11), we obtain the following relations

$$pA(p) = \omega(p)\sin\phi(p),$$

$$C(p) = p(B(p)+1) = \omega(p)\cos\phi(p). \tag{2.23}$$

Now, it is easy to observe that the solution of the equation (2.20) is known once the solution of the equation (2.14) is found. Taking appropriate traces from Eq. (2.20) we obtain the following expressions

$$kA(k) = \tfrac{2}{3}\int\frac{d^3p}{(2\pi)^3}V(\vec{p}-\vec{k})\sin\phi(p),$$

$$kB(k) = (Z-1)k-\tfrac{2}{3}\int\frac{d^3p}{(2\pi)^3}V(\vec{p}-\vec{k})\hat{k}\hat{p}\cos\phi(p). \tag{2.24}$$

Multiplying the first one by $1+B(k)$, the second by $A(k)$ and then subtracting the second equation from the first one we arrive at the Eq. (2.14). Also the quasi-particle energy $\omega(k)$ can be written in terms of $\phi(k)$. Inserting Eq. (2.23) into (2.24) gives

$$\omega(k) = \frac{kA(k)}{\sin\phi(k)} = \tfrac{2}{3}\int \frac{d^3p}{(2\pi)^3} V(\vec{p}-\vec{k}) \frac{\sin\phi(p)}{\sin\phi(k)}. \tag{2.25}$$

By means of the gap equation (2.14) this formula can be converted into the form

$$\omega(k) = k\cos\phi(k) + \tfrac{2}{3}\int \frac{d^3p}{(2\pi)^3} V_L(\vec{p}-\vec{k})(\sin\phi(p)\sin\phi(k) + \hat{k}\hat{p}\cos\phi(p)\cos\phi(k))$$

$$+\tfrac{2}{3}\int \frac{d^3p}{(2\pi)^3} V_c(\vec{p}-\vec{k})(\sin\phi(p)\sin\phi(k) + \hat{k}\hat{p}(\cos\phi(p)-1)\cos\phi(k)). \tag{2.26}$$

Hence, the addition of the Coulomb potential gives finite contribution to the total quasi-particle energy, due to the ultraviolet counter-term added to the kinetic part of the Hamiltonian Eq. (2.1). However, the linear potential term is singular (confining potential), reflecting the unphysical character of $\omega(k)$. From the Eq. (2.25) we can see that the excitation energy $\omega(k)$–$\omega(0)$, which is, in turn, a physical observable, is infrared finite. Since we are going to use the quantity $\omega(k)$–$\omega(0)$ in further calculation we regularize the infinity, by introducing a small cutoff λ around the singular point $p = k$, and taking the $\lambda \to 0$ limit at the end.

Finally, let us comment on the Lorentz vector character of the potential (2.12). This vector character is forced by the chiral symmetry. However, from the experiment we know that the confining quark interaction is predominately Lorentz scalar [18]. Presence of such scalar term in the Hamiltonian would manifestly break the chiral symmetry. A solution of this paradox could be found in the dynamics of the chiral symmetry breaking. An effective Lorentz scalar (mass) term appears already on the one-particle Hamiltonian (H_2) level. Using the gap equation and Eq. (2.10) H_2 can be rewritten in the form

$$H_2 = \sum_{\vec{k},s,\alpha} H(\vec{k})(b^\dagger_{s\alpha}(\vec{k})b_{s\alpha}(\vec{k}) + d^\dagger_{s\alpha}(-\vec{k})d_{s\alpha}(-\vec{k})), \tag{2.27}$$

where

$$H(\vec{k}) = \omega(\vec{k})(\sin\phi(k)\beta + \cos\phi(k)\vec{\alpha}\hat{k}), \tag{2.28}$$

with $\omega(k)$ is given by Eq. (2.26). Presence of the mass (scalar) term formally reflects the nontrivial ($\beta(k) \neq 0$) structure of the vacuum $|\Omega\rangle$.

3. The Bethe-Salpeter equation — the pion properties

A pion, as a bound state 0^{-+} of the massless quark and antiquark is described by the homogeneous Bethe-Salpeter equation [25] (this equation is discussed in the Appendix B and illustrated in Fig. 5b)

$$\mathcal{P}(P,p) = -i\tfrac{4}{3}\int \frac{d^4q}{(2\pi)^4} V(\vec{p}-\vec{q})\gamma^0 S^{(4)}(P+q)\mathcal{P}(P,q)S^{(4)}(P-q)\gamma^C, \tag{3.1}$$

with quark propagator defined by Eq. (2.22a). $\mathscr{P}(P, p)$ is the pion vertex part defined as follows

$$\mathscr{P}_{\alpha\beta}(P, p) = \int \frac{d^4x}{(2\pi)^4} e^{iPX+ipx}\langle\Omega|\mathrm{T}[\psi_\alpha(X+x)\bar{\psi}_\beta(X-x)]\,|\Pi\rangle, \tag{3.2}$$

where $2P$ is the total momentum of the bound state $|\Pi\rangle$ (see App. A), p is the relative quark momentum and X, x are their conjugate coordinates respectively. The bound state amplitude $\mathscr{P}(P, p)$ fulfils the following parity $(-)$ and charge conjugation $(+)$ constraints

$$\mathscr{P}(P, p) = -\gamma^0\mathscr{P}(\tilde{P}, \tilde{p})\gamma^0 \text{ and } \mathscr{P}(P, p) = +C\mathscr{P}(P, -p)C. \tag{3.3}$$

C is the charge conjugation matrix. The operator denoted by $\sim$ transforms a four-vector $(p^0, \vec{p})$ into $(p^0, -\vec{p})$.

It has been shown [6, 7] that the chirally nonsymmetric solution of the gap equation can be used to construct the massless pseudoscalar solution of the Eq. (3.1), with $P = 0$. This can be achieved by performing an infinitesimal chiral rotation applied to the equation (2.20). Let us define (for simplicity we suppress the izospin matrices)

$$\mathscr{P}_0(\vec{p}) = -\frac{i}{2}\frac{d}{d\alpha}(e^{i\alpha\gamma^5}\Sigma(\vec{p})e^{i\alpha\gamma^5})\Big|_{\alpha=0} = pA(p)\gamma^5. \tag{3.4}$$

Performing the same operation on the both sides of the gap equation (2.20) we obtain just the bound state equation (3.1), with $\mathscr{P}_0(\vec{p}) = \mathscr{P}(P = 0, |\vec{p}|, \vec{p})$ obeying the conditions (3.3). It means that spontaneous breaking of the chiral symmetry implies the existence of the Goldstone pion. However, the normalization of the solution $\mathscr{P}_0$ cannot be computed, because in this momentum region (pion at rest) the matrix element $\langle\Pi|\Pi\rangle \sim E(\vec{P}) = 0$, as the pion is massless — $E(\vec{P})$ is the pion energy. In order to calculate the normalization we have to know the wave function for moving pion [7], or for the static one with a small mass ($\mu_\pi \neq 0$) [6]. In this paper we consider the second alternative.

The finite mass of a pion is caused by non-zero mass of current quarks, which explicitly breaks the chiral symmetry. Therefore, we introduce massive quarks to our model, and at the end take the chiral limit. The propagator of a massive quark takes the following form

$$S^{(4)}(p) = \frac{i}{p^0\gamma^0 - \vec{p}\vec{\gamma} - \Sigma(\vec{p}) - m}, \tag{3.5}$$

where $\Sigma(p)$ is given by the Eq. (2.19), with the functions A and B depending on the quark mass. Now, the pion rest frame is well defined and the general form for the $J^{PC} = 0^{-+}$ vertex function, for $\vec{P} = 0$, is the following

$$\mathscr{P}(\mu_\pi, \vec{p}) = \mathscr{P}_\mathrm{p}(p)\gamma^5 + \mu_\pi(\gamma^0\gamma^5\mathscr{P}_\mathrm{A}(p) + \gamma^0\gamma^5\vec{\gamma}\vec{p}\,\mathscr{P}_\mathrm{T}(p)), \tag{3.6}$$

where the functions $\mathscr{P}_\mathrm{p}(\mathscr{P}_0 = \mathscr{P}_\mathrm{p}\gamma^5)$, $\mathscr{P}_\mathrm{A}$ and $\mathscr{P}_\mathrm{T}$ are determined by the Eq. (3.7). Other terms in Eq. (3.6) are forbidden, because of the Lorentz invariance and Eqs. (3.3). Sub-

stituting the expression (3.6) for $\mathscr{P}$ into Eq. (3.1), performing appropriate traces, integration over q^0 and then taking the chiral limit one finds

$$\mathscr{P}_{\mathrm{p}}(p) = pA(p)$$

$$\mathscr{P}_{\mathrm{A}}(p) = \tfrac{2}{3}\int \frac{d^3k}{(2\pi)^3}\, V(\vec{p}-\vec{k}) \sin\phi(k)g(k),$$

$$p\mathscr{P}_{\mathrm{T}}(p) = \tfrac{2}{3}\int \frac{d^3k}{(2\pi)^3}\, V(\vec{p}-\vec{k})]\hat{k}\hat{p} \cos\phi(k)g(k), \tag{3.7}$$

where $g(p)$ is defined as follows

$$g(p) = [\mathscr{P}_{\mathrm{p}}(p)+2p(A(p)\mathscr{P}_{\mathrm{A}}(p)+C(p)p\mathscr{P}_{\mathrm{T}}(p))]/\omega^2(p), \tag{3.8}$$

with $\omega(p)$ given by Eq. (2.26) and $A(p)$ and $C(p)$ by the gap equation (2.20). The function $g(p)$, in turn, is determined by the following integral equation

$$g(p)\omega(p) = \sin\phi(p)+\tfrac{2}{3}\int \frac{d^3k}{(2\pi)^3}\, V(\vec{p}-\vec{k})\,(\sin\phi(p)\sin\phi(k)$$
$$+\hat{k}\hat{p}\cos\phi(p)\cos\phi(k))g(k), \tag{3.9}$$

using the formula, Eq. (2.26), for $\omega(p)$ we obtain the following infrared finite equation

$$g(p)p\cos\phi(p) = \sin\phi(p)$$
$$+\frac{2}{3\pi}\int_0^\infty dkk^2((I_2^{\mathrm{L}}(p,k)\sin\phi(p)\sin\phi(k)+I_1^{\mathrm{L}}(p,k)\cos\phi(p)\cos\phi(k)$$
$$+I_2^{\mathrm{c}}(p,k)\sin\phi(p)\sin\phi(k)+I_1^{\mathrm{c}}(p,k)\cos\phi(p)\cos\phi(k))\,(g(k)-g(p))$$
$$+I_1^{\mathrm{c}}(p,k)\cos\phi(p)g(p)), \tag{3.10}$$

which is then solved numerically. The solution $g(p)$ contains all the information about the bound state. In particular, the pion decay constant is related to the normalization of the pion vertex function $\mathscr{P}$. It is shown in Appendix C that

$$N = -\left[\frac{3}{2\pi^2}\int_0^\infty dkk^2 \sin\phi(k)g(k)\right]^{1/2}. \tag{3.11}$$

It is convenient to choose the normalization factor negative. Substituting the expression for the axial vector current $A_\mu^5(x)\,\bar{\psi}(x)\gamma_\mu\gamma^5\,\psi(x)$ into the definition of the pion decay constant $\langle\Omega|A_\mu^5(0)|\Pi\rangle = -if_\pi P_\mu$ and making use of the Eq. (3.2) we have

$$f_\pi = -N. \tag{3.12}$$

The calculation of the pion charge radius is more complicated. It is obtained following Ref. [6]

$$\langle r_\pi^2 \rangle = 6 \left. \frac{\partial F_\pi(q^2)}{\partial q^2} \right|_{q^2=0}, \tag{3.13}$$

where $F_\pi(q^2)$ is the pion electromagnetic formfactor defined by $\langle Z(P)|J_\mu^{\text{elm}}(0)|Z(P')\rangle = iQ(P_\mu + P'_\mu)F_\pi(q^2)$. Q is the pion charge and $J_\mu^{\text{elm}}(x)$ is the electromagnetic current. Using this definition, the pion formfactor can be expressed in terms of the quark propagator and the pion vertex

$$F_\pi(q^2) = \frac{N_c}{N^2} \frac{1}{E} \int \frac{d^4k}{(2\pi)^4} \operatorname{Tr} [S^{(4)}(k^0 + \tfrac{1}{2}E, \vec{k}) \mathscr{P}(E, \vec{k} + \tfrac{1}{4}\vec{q}) S^{(4)}(k^0 - \tfrac{1}{2}E, k + \tfrac{1}{2}q)\gamma^0$$

$$\times S^{(4)}(k^0 - \tfrac{1}{2}E, \vec{k} - \tfrac{1}{2}\vec{q}) \mathscr{P}(-E, \vec{k} - \tfrac{1}{4}\vec{q})]. \tag{3.14}$$

Inserting Eq. (3.14) into Eq. (3.13) we obtain after straightforward but tedious calculations ($N_c = 3$)

$$\langle r_\pi^2 \rangle = -\frac{1}{N^2} \int_0^\infty \frac{dk}{(2\pi)^2} f(k), \tag{3.15}$$

where the function $f(k)$ is derived in Appendix C.

4. Restoration of the chiral symmetry

The chiral symmetry is expected to be restored at large temperature and density. Since QCD is much too complicated theory to resolve this problem several models have been developed [10, 22]. The present model has also been applied to describe the transition from the low energy broken symmetry phase to the chirally symmetric one — the quark--gluon plasma [11, 12, 13, 20]. In this Chapter we extend the analysis of Refs [12, 13] by including the Coulomb interaction.

In this model nonzero baryonic density may be simply achieved [12, 13]. The whole construction [13] is done in quasiparticle basis. The prototype of the nuclear matter is built from colour singlet baryons containing three valence/constituent quarks, which fill Fermi sea up to a given Fermi momentum K_F.

$$|B\rangle = \prod_{\substack{s_1 s_2 s_3 \\ |\vec{k}| < K_F}} \frac{1}{3!} (b_{s_1 a}^\dagger(\vec{k}) b_{s_2 b}^\dagger(\vec{k}) b_{s_3 c}^\dagger(\vec{k}) \varepsilon_{abc}) |\Omega\rangle, \tag{4.1}$$

with $|\Omega\rangle$ and $b_{as}^\dagger(\vec{k})$ defined by (2.4) and (2.6) respectively. We did not have to introduce the chemical potential into the description since baryonic number is a constant of motion and we work at zero temperature. This construction of the baryonic background has the

good feature that the state $|B\rangle$ automatically represents the sector in Hilbert space with a finite baryonic number density because [13]

$$\varrho_B = \frac{\sigma_f}{3}\frac{K_F^3}{6\pi^2}, \tag{4.2}$$

where $\sigma_f = 2\,(\text{spin}) \times N_f\,(\text{flavour}) \times N_c\,(\text{colour})$ and equals six (twelve) for one (two) flavour (s). This relation (4.2) is very useful because this allows us to directly see the influence of ϱ_B on the chiral symmetry breaking. From the Eq. (4.1) and the definition of the state $|\Omega\rangle$ we see that the introduction of baryons causes the suppression of the $q\bar{q}$ pairs momentum modes below K_F. It occurs due to the Pauli blocking. Introduction of a quark with momentum $\vec{k}$ destroys the pair with this momentum in the vacuum state $|\Omega\rangle$ [3] since

$$b^\dagger_{s3\alpha}(\vec{k})\left(\cos\frac{\phi(k)}{2} - s\tau\sin\frac{\phi(k)}{2}\, b^{0\dagger}_{s\alpha}(\vec{k}) d^{0\dagger}_{s\alpha}(-\vec{k})\right)|0\rangle$$

$$= \left(\cos\frac{\phi(k)}{2}\, b^{0\dagger}_{s\alpha}(\vec{k}) + s\sin\frac{\phi(k)}{2}\, d^0_{s\alpha}(-\vec{k})\right)$$

$$\times\left(\cos\frac{\phi(k)}{2} - s\tau\sin\frac{\phi(k)}{2}\, b^{0\dagger}_{s\alpha}(\vec{k}) d^{0\dagger}_{s\alpha}(-\vec{k})\right)|0\rangle = b^{0\dagger}_{s\alpha}(\vec{k})\,|0\rangle. \tag{4.3}$$

Hence, the baryonic background changes the gap equation and the equation for the pion vertex in the following way

$$k\sin\phi(k) = \frac{2}{3\pi}\int_{K_F}^{\infty} dp(I_2^L(k,p)\sin\phi(p)\cos\phi(k) - I_1^L(k,p)\sin\phi(k)\cos\phi(p))$$

$$+\frac{2}{3\pi}\int_{K_F}^{\infty} dp\left(I_2^c(k,p)\sin\phi(p)\cos\phi(k) + 2I_1^c(k,p)\sin\phi(k)\sin^2\frac{\phi(p)}{2}\right), \tag{4.4}$$

and

$$g(k)k\cos\phi(k) = \sin\phi(k)$$

$$+\frac{2}{3\pi}\int_{K_F}^{\infty} dpp^2((I_2^L(k,p)\sin\phi(k)\sin\phi(p) + I_1^L(k,p)\cos\phi(k)\cos\phi(p)$$

$$+I_2^c(k,p)\sin\phi(k)\sin\phi(p) + I_1^c(k,p)\cos\phi(k)\cos\phi(p))\,(g(p) - g(k))$$

$$+I_1^c(k,p)\cos\phi(k)g(k)). \tag{4.5}$$

[3] For a more detailed analysis see Ref. [13].

The suppression of the small momenta in the integration over p in Eqs. (4.4), (4.5) can also be demonstrated from the Green function analysis. This was done in Ref. [12]. The suppression does not damage the infrared and ultraviolet finiteness of the gap equation and the pion vertex equation, as the Coulomb potential appears here in the same way as in the Eqs. (2.17), (3.10).

Equations (4.4) and (4.5) allow us to see the effect of the Coulomb potential on the chiral parameters with nonzero baryonic number density, which is discussed in the following section.

5. Numerical solutions

Now, before the numerical results are shown, let us briefly summarize the overrelaxed Gauss-Seidel algorithm, which is used to solve the gap equation and the Bethe-Salpeter equation for a pion. A detailed description of the method is presented in Ref. [14].

5.1. Gauss-Seidel algorithm

In order to solve numerically the gap equation

$$k \sin \phi(k) = \frac{2}{3\pi} \int_0^\infty dp (I_2^{\mathrm{L}}(k, p) \sin \phi(p) \cos \phi(k) - I_1^{\mathrm{L}}(k, p) \sin \phi(k) \cos \phi(p))$$

$$+ \frac{2}{3\pi} \int_0^\infty dp \left(I_2^{\mathrm{C}}(k, p) \sin \phi(p) \cos \phi(k) + 2 I_1^{\mathrm{C}}(k, p) \sin \phi(k) \sin^2 \frac{\phi(p)}{2} \right), \tag{5.1}$$

with functions $I^{\mathrm{L}}_{(1,2)}(k, p)$, $I^{\mathrm{C}}_{(1,2)}(k,)$ given by Eq. (2.18), it is convenient to replace the continuum variables k, p in the following way: $k_i = 2di$ and $p_i = 2di - d$, $i = 1, \ldots, N$, where $2d$ is the distance between neighboring points. After discretization we rewrite the Eq. (5.1) in the form

$$C_1 \sin \phi(k_i) + C_2 \sin \phi(k_i) \cos \phi(k_i) + C_3 \cos \phi(k_i) = 0, \tag{5.2}$$

for $i = 1, \ldots, N$. The coefficients $C_{(1,2,3)}$ depend on $\phi(p_j)$ in the following way

$$C_1 = \frac{2}{3\pi} \sum_{j=1^\lambda}^{N} 2d \left(-I_1^{\mathrm{L}}(k_i, p_j) \cos \phi(p_j) + 2 I_1^{\mathrm{C}}(k_i, p_j) \sin^2 \frac{\phi(p_j)}{2} \right) - k_i, \tag{5.3a}$$

$$C_2 = \frac{2}{3\pi} \int_{k_i - \lambda}^{k_i - \lambda} dp p^2 (I_2^{\mathrm{L}}(k_i, p_j) - I_1^{\mathrm{L}}(k_i, p_j)), \tag{5.3b}$$

$$C_3 = \frac{2}{3\pi} \sum_{j=1^\lambda}^{N} 2d (I_2^{\mathrm{L}}(k_i, p_j) + I_2^{\mathrm{C}}(k_i, p_j)) \sin \phi(p_j). \tag{5.3c}$$

The second term in Eq. (5.2) arises from the p-integration over a small neighborhood of k_i — say, over range $\{k_i-\lambda, k_i+\lambda\}$, where $\lambda < d$. This singles out the infrared singularity at $p = k$ from $C_{(1,3)}$, which occurs due to the presence of the linear potential. Both singular terms in C_1 and C_3 cancel at that point producing finite limit. The integration over p in Eq. (5.1) is replaced by the sum $\sum_\lambda$, where the index λ implies omission of the terms from integral (5.3b).

The Gauss-Seidel iteration consists of the successive replacement of each mode $\phi(k_i)$ by $\phi^{GS}(k_i)$, which solves the Eq. (5.2), as a function of a single variable $\phi(k_i)$, with other variables $\phi(k_{j\neq i})$ held fixed. An initial guess $\phi^0(k)$, obeying suitable boundary conditions, has to be supplied as an input to the algorithm. Boundary conditions can be derived from the integral equation (5.1). After setting $k = 0$, the gap equation reduces to $\cos\phi(0) = 0$, which gives

$$\phi(0) = \frac{\pi}{2}. \tag{5.4}$$

Expanding the r.h.s. of Eq. (5.1) gives the large-k behaviour of the gap function $\phi(k)$

$$\phi(k \to \infty) \sim \frac{V(k)}{k}, \tag{5.5}$$

which yields, with the aid of Eq. (2.13)

$$\phi(k \to \infty) \to \frac{b}{k^3}, \tag{5.6}$$

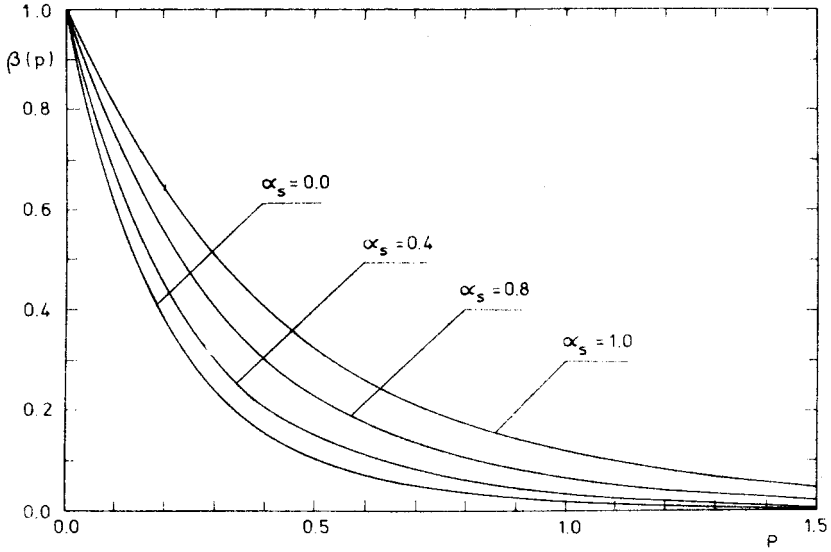

Fig. 1. The function $\beta(k) = \tan\dfrac{\phi(k)}{2}$ for several values of α_s

for the Coulomb potential. The Eqs. (5.2) for $\phi(k_i)$ are solved using Newton iterations. It is more efficient to update the function $\phi(k_i)$ in the following way

$$\phi(k_i) \to \phi^{\mathrm{rGS}}(k_i) = \omega\phi^{\mathrm{GS}}(k_i)+(1-\omega)\phi(k_i), \tag{5.7}$$

where ω is the relaxation parameter, which can be determined for a coarse mesh (say, 40 points). In our case $\omega_0 = 1.93$. The introduction of the relaxation parameter yields (about seven times) more efficient algorithm. This allows for the faster convergence, after passing to larger lattices.

After several iterations with $\omega = 1$ and many iterations (about two hundred sweeps) with $\omega = \omega_0$ we obtain the solution for $\phi(k)$, which is depicted in Fig. 1 for some values of α_s. In the case of the linear potential ($\alpha_s = 0$) the momentum space wave function behaves like $1/k^5$ for large k (see Eq. (5.5)). After the introduction of the Coulomb potential the large-k asymptotic behaviour is replaced by (5.6), which will be important in the next chapter.

5.2. Chiral parameters

At first, let us calculate the dynamical quark mass m^*. It is related to the small momentum behaviour of the gap function

$$\phi(k) \sim \frac{\pi}{2} - ak. \tag{5.8}$$

Expanding the $\Lambda_+(\vec{k})$ near $k = 0$ gives

$$\Lambda_+(\vec{k}) = \tfrac{1}{2}(1+\beta+a\vec{\alpha}\vec{k}). \tag{5.9}$$

Comparing the expression (5.9) with the massive particle propagator

$$\tfrac{1}{2}\left(1+\beta+\frac{1}{m^*}\vec{\alpha}\vec{k}\right), \tag{5.10}$$

we obtain

$$m^* = \frac{1}{a} = -\left(\frac{d\phi}{dk}\right)_{k=0}. \tag{5.11}$$

The calculation of the quark condensate was presented in Ref. [21]. As $\langle\Omega|\bar{\psi}\psi|\Omega\rangle$ is logarithmically divergent the quark condensate needs renormalization. To this end, we renormalize the wave function $\psi \to \psi/\sqrt{Z}$, where Z is given by Eq. (2.16) and then, after introduction a temporary ultraviolet momentum cutoff Λ we compute the quark condensate using the definitions (2.4) and (2.8)

$$\langle\bar{u}u\rangle = \frac{1}{Z}\langle\Omega|\bar{\psi}\psi|\Omega\rangle, \tag{5.12}$$

then, taking the $\Lambda \to \infty$ we obtain

$$\langle\bar{u}u\rangle = -\frac{27}{8\pi}\frac{b}{\alpha_s}, \tag{5.13}$$

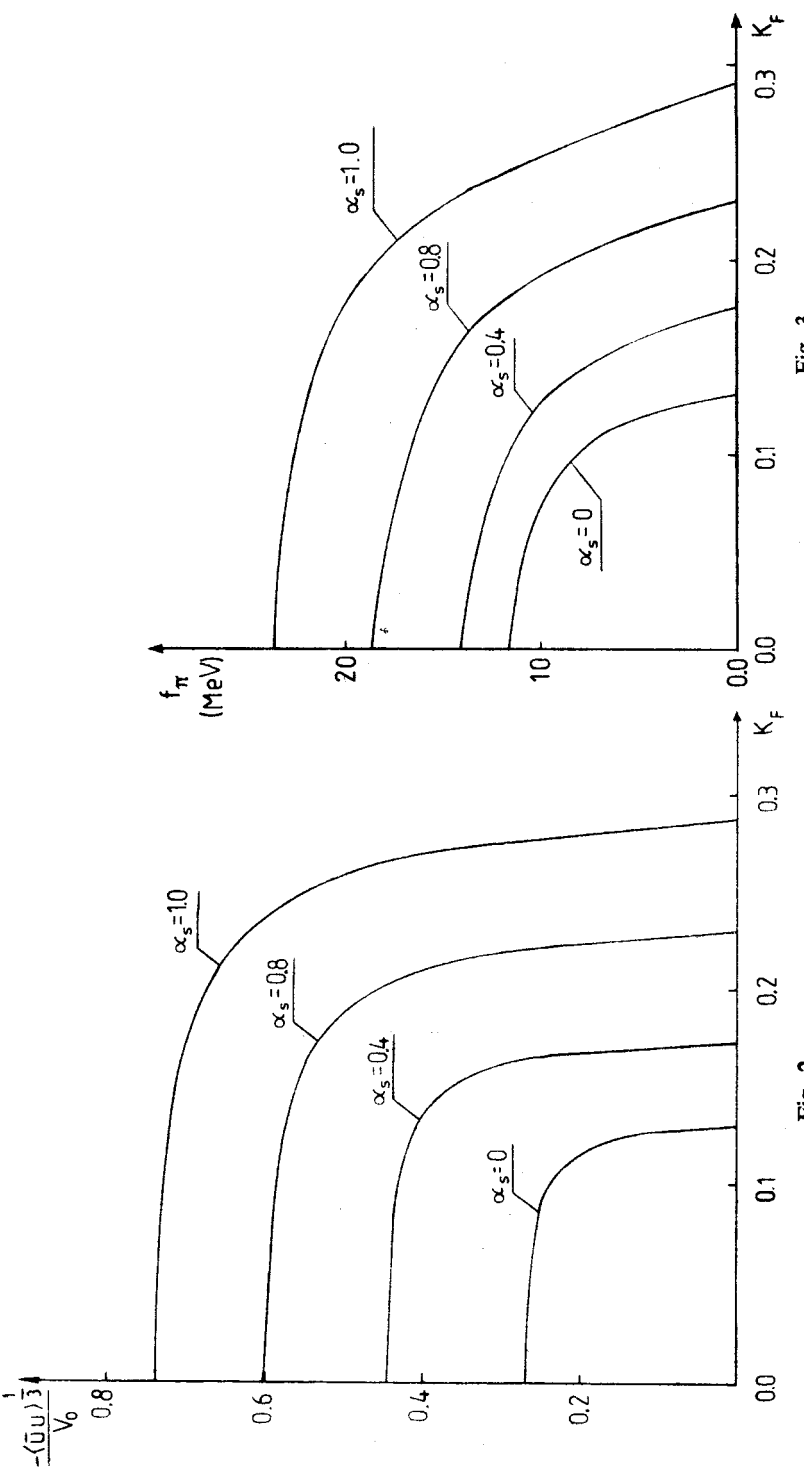

Fig. 2

Fig. 3

Fig. 2. The K_F dependence of the quark condensate (see Eq. (5.10)) for various α_s

Fig. 3. The pion decay constant versus K_F for various values of α_s

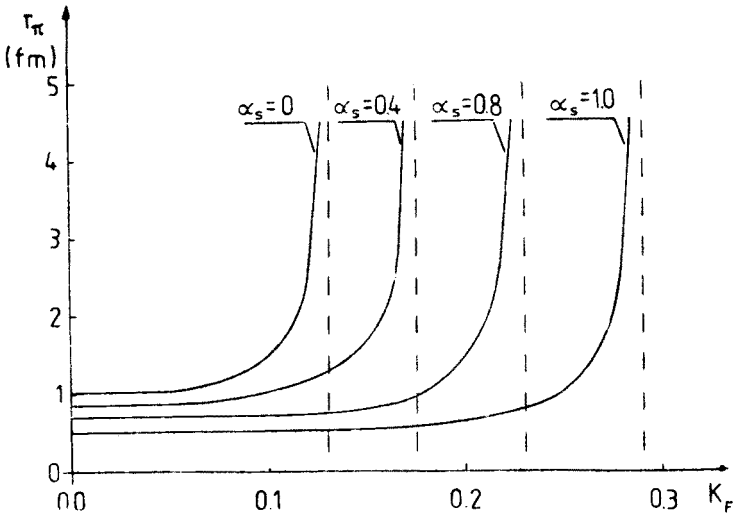

Fig. 4. The pion charge radius plotted versus K_F for some values of α_s, as obtained from Eqs. (3.15) and (C5)

TABLE

The quark condensate $\langle\bar{u}u\rangle$, dynamical quark mass m^*, density of quark pairs ϱ (see Eq. (5.12)), energy gap ΔE (see Eq. (5.11)), the pion decay constant f_π and the pion charge radius for some values of α_s. At the bottom we quote the experimental values taken from indicated references

α_s	$\langle\bar{u}u\rangle$ (MeV^3)	m^* (MeV)	ΔE (MeV^4)	ϱ (MeV^3)	f_π (MeV)	r_π (fm)
0.0	$-(95)^3$	70	$-(88)^4$	$(41)^3$	11	1.03
0.4	$-(150)^3$	95	$-(97)^4$	$(49)^3$	14	0.87
0.8	$-(210)^3$	120	$-(115)^4$	$(65)^3$	19	0.64
1.0	$-(260)^3$	170	$-(136)^4$	$(81)^3$	24	0.49
exp.	$-(225)^3$ [15]	300 [15]	$-(140)^4$ [17]	—	93 [1]	0.68 [24]

where b is defined in Eq. (5.6). Applying the Eqs (5.11), (5.13) we calculated $\langle\bar{u}u\rangle$ and m^* for some values of α_s — see Table I. The string tension was taken to be $\sqrt{\sigma} = 350$ MeV.

The energy difference between the chirally symmetric and broken phases and the density of quark-antiquark pairs in the vacuum state can be calculated form the following formulas

$$\Delta E = \mathscr{E}[\phi(k) \equiv 0] - \mathscr{E}[\phi(k)] = 2N_c N_f \int \frac{d^3k}{(2\pi)^3} (\omega^0(k) - \omega(k)) \frac{1-\cos\phi(k)}{2}, \quad (5.14)$$

$$\varrho = 2N_c N_f \int \frac{d^3k}{(2\pi)^3} \frac{1-\cos\phi(k)}{2}, \quad (5.15)$$

where $\omega^0(k)$ is given by Eq. (2.26) with $\phi(k) = 0$ and the vacuum energy $\mathscr{E}[\phi(k)]$ follows from Eq. (2.10). ΔE and ϱ are shown in Table I. Once the solution of the gap equation $\phi(k)$ is known it is easy to find the pion vertex $g(k)$ solving Eq. (3.10) by means of the same algorithm. Though $\phi(k_i)$ is the input function in the equation for pion vertex, the numerical

errors are small and do not influence the accuracy of the solution for the pion wave function $g(k_i)$ very much. With the aid of equations (3.12) and (3.14) we can obtain the values of the pion decay constant and the pion radius. The results are presented also in Table I. The influence of the baryonic number density on quark condensate in the presence of the Coulomb potential is illustrated in Fig. 2. The K_F dependence of the pion decay constant and the pion radius is depicted in Fig. 3 and Fig. 4 respectively.

6. *Discussion*

From the results presented in Section V it is evident that the introduction of the Coulomb potential makes the model more realistic. This confirms the earlier expectations [7, 9, 12]. The common improvement in all parameters listed in Table I can be clearly understood. From the formula for potential (2.13), it follows that the addition of the Coulomb field to the linear one effectively makes the string tension larger at small distances (both interactions in Eq. (2.13) have the same sign). The increase of the string tension produces more physical chiral parameters. Better description of the chiral symmetry breaking results from the high momentum components in the potential. Hence, this effect is due to the contribution from small Cooper pairs — we see from Fig. 1 that the condensate of quark-antiquark pairs becomes more dense after introduction of the Coulomb potential.

The quark condensate, the energy shift between the chiral symmetric and broken phases ΔE (the latter we compare with the bag constant $B = (140\ \text{MeV})^4$ [17]) and the pion radius are rather in agreement with the experiment. However, the pion decay constant f_π and the constituent quark mass are still too small. Similar results have been obtained by other authors [6, 7, 20]. In the most recent study of the problem by Alkofer and Amundsen [20] the chiral parameters are calculated for the temperature dependent Richardson potential

$$V(q) = -\frac{\alpha(q, T)}{q^2}, \quad \text{with} \quad \alpha(q, T) = \frac{12\pi}{(11N_c - 2N_f)\ln(1 + aT^2 + q^2/\Lambda^2)}.$$

The potential reduces (for $T = 0$) to the linear one for small q^2 and to the Coulomb potential for large momentum. This approach is complementary to our in two respects. First, the authors of Ref. [20] are probing different kind of potential. The quark interaction is only known for large momentum — relevant for charmonium physics. Therefore, it is important to see how much the chiral parameters are sensitive to the shape of potential for small momentum. Secondly, they analyze the chiral symmetry breaking at finite temperature. Solving the gap equation and the equation for the pion vertex renormalized in the way suggested by Adler and Davis [9] they obtain the T-dependence of the quark mass m^* and the pion decay constant f_π. The calculations were carried out at zero baryonic density. Therefore, we can compare them with our results only in the limit $T = 0$ and $K_F = 0$. In Ref. [20] the experimental value of the quark mass $m^* = 300$ MeV is used to fix the only (at $T = 0$) parameter Λ in the Richardson potential. After solving the equation for $g(k)$ they have obtained pion decay constant $f_\pi = 58$ MeV — also considerably lower than the experimental one. Furthermore, for the same value $\Lambda = 1800$ MeV they find

$\Delta E = (300\ \text{MeV})^4$ and $\varrho = (230\ \text{MeV})^3$. In order to have better comparison with Ref. [20], we have solved the equation for the pion vertex $g(k)$, with $\phi(k)$ reproducing the experimental value $m^* = 300$ MeV and found similar pion decay constant $f_\pi = 47$ MeV and $\Delta E = (370\ \text{MeV})^4$, $\varrho = (180\ \text{MeV})^3$. This comparison implies that the chiral parameters do not depend strongly on the kind of potential utilized. The results also suggest that the small value of f_π from Table I is not only due to the incorrect shape of the gap function $\phi(k)$.

The discrepancies in the pion decay constant f_π and the constituent quark mass may result from the lack of the transverse gluons and retardation effects, which are difficult to study [18]. The situation is similar to that in superconductivity. Not only the Coulomb potential is required besides the long range BCS interaction, but the retardation effects are needed to obtain a quantitative agreement with the experiment for a number of superconductors [19].

The influence of the Coulomb potential on the values of chiral parameters in the presence of the baryonic background, is illustrated in Figs. 2, 3, 4. The K_F (hence the baryon density) dependence of the parameters depicted in these figures can be understood from the formula (4.1). As discussed in Section 4 the introduction of a quark with momentum $\vec{k}$ destroys the pair in $|\Omega\rangle$ with quark internal momentum $\vec{k}$ (Pauli blocking). Hence the role of the large momentum components is enhanced accordingly. In the large momentum limit the kinetic energy dominates over the self-energy. Therefore, the instability condition (see introduction) suggests that the chiral symmetry should be restored for some $K_F = K_F^C$. This is confirmed by the numerical calculation. From Fig. 2 we see that for $\alpha_s = 0$ we have $K_F^C = 46$ MeV, with $V_0 = 350$ MeV. This result was obtained in Ref. [12, 13]. With the Coulomb potential K_F^C is shifted to the value 100 MeV (or $\varrho_B^C = (60\ \text{MeV})^3$), for $\alpha_s = 1$. The recovery of the chiral symmetry in this model, supports the lattice and the mean field calculations [10]. However, resulting critical value for Fermi momentum is still smaller then the generally expected $K_{F\,exp}^C = 450$ MeV (or $\varrho_B^C = (270\ \text{MeV})^3$) [22]. Is not clear whether the instantaneous interaction or the simple way of achieving the nonzero baryonic number density is the reason for the discrepancy. Another possible origin of the trouble would come from the vector character of the confining potential which, as data shows, is predominatly Lorentz scalar [18]. Unfortunately, a Lorentz scalar instantaneous potential would explicitly break the chiral symmetry. For this reason it is not present in the original Hamiltonian. However, an effective Lorentz *scalar* term (which is also needed in the spectroscopy) could originate from dynamics of the chiral symmetry breaking. In fact this happens in our approach on the level of the one particle Hamiltonian — see Eq. (2.28). The detailed study of the problem is now in progress.

From Fig. 2 we conclude that the restoration of the chiral symmetry occurs through the second order phase transition. This observation seems to be in disagreement with Ref. [13], where the first order phase transition has been reported. However, in the approach of Ref. [13], we have performed the linearized approximation in $\phi(k)$. Hence, the discrepancy is the result of this approximation. It would be interesting to observe, how other approximations, which are performed there, influence the order of the phase transition. Our prediction concerning the order of the chiral phase transition is in contrast to the earlier lattice calculation [10], where the first order phase transition was found (for SU(3) gauge

theory at zero temperature). However, the introduction of baryons on a lattice encounters many difficulties [27], and the result is still rather preliminary.

Another interesting result, which confirms our intuitive understanding of the chiral symmetry breaking in QCD, is shown in Fig. 4. After increasing baryonic number density the pion radius increases, to become infinite for $K_F = K_F^C$. Thus the recovery of the chiral symmetry is associated with the vanishing of the pion, as expected for the Goldstone boson. The Coulomb potential shifts the value of the critical momentum K_F^C.

The K_F-behaviour of pion radius also supports the general hypothesis, that the size of a quark bound state (e.g. nucleon) becomes larger after immersing it into the baryonic environment. This postulate was used phenomenologically to explain the EMC effect [23]. Now, it is possible to make this connection more quantitative.

In conclusion, the present model seems to give a satisfactory description of the chiral symmetry in QCD. Most of the chiral parameters became more realistic after inclusion of the Coulomb potential. However, further improvements are necessary. In particular, it will be crucial to understand the significance of the time dependence in the model. Though the problem is very complicated, the analogy to the superconductivity model seems to be promising.

The author would like to thank Prof. A. Białas for introducing me to the model and dr. J. Wosiek for many stimulating discussions. I also would like to thank Mr. W. Kubica, University of Rochester NY, USA and A. von Humbold Fundation, W. Germany, for the computer assistance which made this publication possible.

APPENDIX A

The renormalized gap equation in the Coulomb gauge

Analogously to the theory of superconductivity, the gap equation follows from the Schwinger-Dyson equations for the quark propagator and the quark-gluon vertex part [9]. This derivation allows us to perform correct renormalization and see clearly which approximation leads to our equation (2.20). The renormalized vertex equations for vector (Γ_μ) and axial-vector (Γ_μ^5) vertices, after omission of the fermion annihilation diagrams, are

$$\Gamma_\mu(p, p')_{\delta\gamma} = (Z\gamma_\mu)_{\delta\gamma} + \int \frac{d^4q}{(2\pi)^4} [iS^{(4)}(p'+q)\Gamma_\mu(p'+q, p+q)iS^{(4)}(p+q)]_{\beta\alpha} \times K_{\alpha\beta,\gamma\delta}(p+q, p'+q, q), \tag{A1a}$$

$$\Gamma_\mu^5(p, p')_{\delta\gamma} = (Z\gamma_\mu\gamma^5)_{\delta\gamma} + \int \frac{d^4q}{(2\pi)^4} [iS^{(4)}(p'+q)\Gamma_\mu^5(p'+q, p+q)iS^{(4)}(p+q)]_{\beta\alpha} \times K_{\alpha\beta,\gamma\delta}(p+q, p'+q, q), \tag{A1b}$$

where $K(p+q, p'+q, q)$ is the quark-antiquark Bethe-Salpeter kernel. In ladder approximation, which is imposed here after theory of heavy quarks bound states [26], one sets

$$K_{\alpha\beta,\gamma\delta}(p+q, p'+q, q) = -i\gamma^0_{\alpha\gamma}\tfrac{4}{3}V(\vec{q})\gamma^0_{\beta\delta}. \tag{A2}$$

Using the Ward identities

$$(p'-p)^{\mu}\Gamma_{\mu}(p', p) = S^{(4)-1}(p)-S^{(4)-1}(p'),$$
$$(p'-p)^{\mu}\Gamma^{5}_{\mu}(p', p) = \gamma^{5}S^{(4)-1}(p)+S^{(4)-1}(p')\gamma^{5} \tag{A3}$$

we obtain from Eq. (A1a, b)

$$(p'-p)^{\mu}\Gamma_{\mu}(p', p) = (Z\gamma_{\mu})(p'-p)^{\mu}-\int\frac{d^4q}{(2\pi)^4}\, i\,\tfrac{4}{3}\, V(\vec{q})\gamma^0[iS^{(4)}(p'+q)$$
$$\times[S^{(4)-1}(p'+q)-S^{(4)-1}(p+q)]iS^{(4)}(p'+q)]\gamma^0$$
$$= (Z\gamma_{\mu})p'^{\mu}-\int\frac{d^4q}{(2\pi)^4}\, i\,\tfrac{4}{3}\, V(\vec{q})\gamma^0 iS^{(4)}(p'+q)\gamma^0$$
$$-(Z\gamma_{\mu})p'^{\mu}+\int\frac{d^4q}{(2\pi)^4}\, i\,\tfrac{4}{3}\, V(\vec{q})\gamma^0 iS^{(4)}(p'+q)\gamma^0 = S^{(4)-1}(p)-S^{(4)-1}(p'). \tag{A4}$$

Similar equation to Eq. (A4) can be derived from the second formula of Eq. (A3). As the p, p'-dependences in (A4) separate we have

$$S^{(4)-1}(p) = (Z\gamma_{\mu})p'^{\mu}-\int\frac{d^4q}{(2\pi)^4}\, i\,\tfrac{4}{3}\, V(\vec{q})\gamma^0 iS^{(4)}(p'+q)\gamma^0. \tag{A5}$$

The non-relativistic ansatz (4.1) for the self-energy yields

$$\Sigma(\vec{p}) = (Z_0-1)p^0\gamma^0+(Z-1)\vec{p}\cdot\vec{\gamma}+\frac{1}{6\pi^3}\int d^3qV(\vec{p}-\vec{q})\gamma^0 S^{(3)}(\vec{q})\gamma^0, \tag{A6}$$

where we have integrated out q^0 in the Eq. (A5). Since the Bethe-Salpeter kernel does not depend on time, Γ_0 can be easily determined. From Eq. (A1a) we see, by direct calculation, that $\Gamma_0(p, p')$ is equal to $Z_0\gamma^0$. It follows from the asymptotic freedom that, in the large momentum limit, the quark-gluon vertex is equal to γ^0. This condition sets $Z_0 = 1$. Substituting the value of Z_0 into Eq. (A6) gives Eq. (2.20) from Section 4.

APPENDIX B

The Bethe-Salpeter equation — normalization

In this section we present the derivation of the homogeneous Bethe-Salpeter equation (BSE) (3.1), following Refs. [7, 25]. To this end, we start with the inhomogeneous BSE for the four point Green function (G), which can be symbolically written ($G_0 = S_1S_2$)

$$G = G_0+G_0\, KG, \tag{B1}$$

where K is given by Eq. (A2). With the notation introduced in Fig. 5, Eq. (B1) reads

$$G_{\sigma_1\sigma_2,\sigma_3\sigma_4}(p_1, p_2; p_3, p_4) = S^{(4)}_{\sigma_1\sigma_3}(p_1)S^{(4)}_{\sigma_2\sigma_4}(p_2)$$

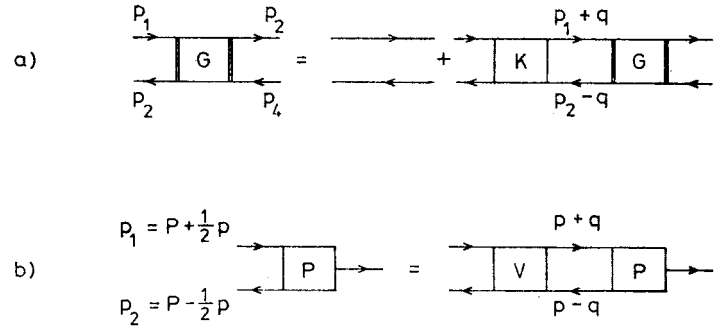

Fig. 5. Graphical illustration of the Bethe-Salpeter equation, a) Eq. (B1), b) Eq. (B4)

$$+\int \frac{d^4q}{(2\pi)^4}\tilde{K}_{\sigma_1\sigma_2,\sigma_5\sigma_6}(p_1, p_2, q)i\tilde{S}^{(4)}_{\sigma_5\sigma_7}(p_1+q)i\tilde{S}^{(4)}_{\sigma_6\sigma_8}(p_2-q)$$

$$\times \tilde{G}_{\sigma_7\sigma_8,\sigma_3\sigma_4}(p_1+q, p_2-q; p_3, p_4). \tag{B2}$$

Assuming existence of a bound state formed from the scattered particles we can rewrite the two body propagator (around the pole) in the following way

$$\tilde{G}_{\sigma_1\sigma_2,\sigma_3\sigma_4}(p_1, p_2; p_3, p_4) = \frac{\mathscr{P}(P, p)\bar{\mathscr{P}}(P, p)}{((2P)^2-E_Z^2)}, \tag{B3}$$

where $2P = p_1-p_2$ and $2p = p_1+p_2$ are the center mass and relative momenta respectively, E_Z is the energy of the bound state. After inserting Eq. (B3) into Eq. (B2), recalling the ladder approximation Eq. (A2) and changing variables we obtain the homogeneous BSE for the bound state vertex part

$$\mathscr{P}(P, p) = -i\tfrac{4}{3}\int \frac{d^4q}{(2\pi)^4} V(\vec{p}-\vec{q})\gamma^0 S^{(4)}(P-q)\mathscr{P}(P, q)S^{(4)}(P+q)\gamma^0, \tag{B4}$$

with the quark propagator defined by Eq. (2.22a). Using the definition of the four point Green function the bound state amplitude $\mathscr{P}(P, p)$ can be related to the time ordered product of the quark fields [25]

$$\mathscr{P}_{\alpha\beta}(P, p) = \int \frac{d^4x_1}{(2\pi)^4} e^{iP(x+y)+ip(x-y)}\langle\Omega|\mathrm{T}[\psi_\alpha(x)\bar{\psi}_\beta(y)]\,|\Pi\rangle. \tag{B5}$$

To derive the normalization condition we rewrite BSE (B1) in the following form

$$G(G_0^{-1}-K)G = G. \tag{B6}$$

Comparing the residues at the pole P_0 and using the homogeneous BSE (B4) we arrive at the equation (3.11). For more details see Ref. [7]. Another derivation of the normalization factor N is presented in Appendix C.

APPENDIX C

The pion charge radius

The pion charge radius is defined by [6]

$$\langle r_\pi^2 \rangle = 6 \left. \frac{\partial F_\pi(q^2)}{\partial q^2} \right|_{q^2=0}, \tag{C1}$$

where $F_\pi(q^2)$ is the pion electromagnetic formfactor

$$\langle \Pi(P)| J_\mu^{\text{elm}}(0) |\Pi(P')\rangle = iQ(P_\mu + P'_\mu)F_\pi(q^2). \tag{C2}$$

Q is the pion charge, and

$$J_\mu^{\text{elm}}(x) = \bar{\psi}(x)\gamma_\mu\psi(x) \tag{C3}$$

is the electromagnetic current. The pion formfactor, written in terms of the quark propagators and the pion vertex takes the form (3.13). $F(q^2)$ is normalized to $F(0) = 1$. This condition sets the normalization constant N^2. On the other hand, expanding the integrand in Eq. (3.13) for small q^2, performing the trace and inserting the result into (C1) we obtain (after taking the chiral limit and $\lambda \to 0$)

$$\langle r_\pi^2 \rangle = -\frac{1}{N^2} \int_0^\infty \frac{dk}{(2\pi)^2} f(k), \tag{C4}$$

where

$$\begin{aligned}
f(k) = {} & 2k^4 \mathrm{SG}(k) \sin\phi(k) \left(-\sin\phi(k)\,(\phi'(k))^2 + \cos\phi(k)\phi''(k)\right) \\
& + k^2 \cos\phi(k)\phi'(k) \left[-12\mathrm{SG}(k)\mathrm{SP}(k)\right. \\
& - 4k^2 \sin\phi(k)\mathrm{SG}'(k) + 12\mathrm{SG}(k)\sin\phi(k)\,(\cos\phi(k)\mathrm{CP}(k) \\
& \left. + \sin\phi(k)\mathrm{SP}(k)) + 3\mathrm{SG}(k)\sin\phi(k)\right] \\
& + \sin\phi(k) \left[4\mathrm{SG}(k)\mathrm{AA}(k) + 12k^2\mathrm{SG}'(k)\mathrm{SP}(k) + 2k^4\mathrm{SG}''(k)\sin\phi(k)\right. \\
& + 4\mathrm{SG}(k)\sin\phi(k)\,(-3\cos\phi(k)\mathrm{CC}(k) \\
& - 3\sin\phi(k)\mathrm{AA}(k) + \mathrm{CP}^2(k) - 9\mathrm{SP}^2(k)) \\
& - 40\mathrm{SG}(k)\sin^2\phi(k)\,(\sin\phi(k)\mathrm{CP}^2(k) \\
& - 2\mathrm{SP}(k)\cos\phi(k)\mathrm{CP}(k) - \sin\phi(k)\mathrm{SP}^2(k)) \\
& + 10\mathrm{SG}(k)\mathrm{SP}(k) + 3k^2\mathrm{SG}'(k)\sin\phi(k) \\
& - 26\mathrm{SG}(k)\sin\phi(k)\,(\cos\phi(k)\mathrm{CP}(k) + \sin\phi(k)\mathrm{SP}(k)) \\
& \left. - \mathrm{SG}(k)\sin\phi(k)\,(15 - 12\sin^2\phi(k))\right]
\end{aligned}$$

$$+2\mathrm{CG}(k)\cos\phi(k)k^4(-\sin\phi(k)(\phi'(k))^2+\cos\phi(k)\phi''(k))$$

$$+k^2\cos\phi(k)\phi'(k)[-4\cos\phi(k)(k^2\mathrm{CG}'(k)-\tfrac{1}{2}\mathrm{CG}(k))$$

$$-12\sin\phi(k)\mathrm{CG}(k)(\sin\phi(k)\mathrm{CP}(k)-\mathrm{SP}(k)\cos\phi(k))+\cos\phi(k)\mathrm{CG}(k)]$$

$$+\sin\phi(k)\Bigg[-8\mathrm{CG}(k)\mathrm{CC}(k)+2k^5\left(\frac{\mathrm{CG}(k)}{k}\right)''\cos\phi(k)$$

$$+\mathrm{CG}(k)(12\sin^2\phi(k)\mathrm{CC}(k)+4\cos\phi(k)\mathrm{CP}^2(k))$$

$$-16\mathrm{CG}(k)\mathrm{CP}(k)+5(k^2\mathrm{CG}'(k)-\tfrac{1}{2}\mathrm{CG}(k))\cos\phi(k)$$

$$+32\sin\phi(k)\mathrm{CG}(k)(\sin\phi(k)\mathrm{CP}(k)-\mathrm{SP}(k)\cos\phi(k))$$

$$+\cos\phi(k)\mathrm{CG}(k)(12\sin^2\phi(k)-11)\Bigg], \tag{C5}$$

with the functions

$$\mathrm{SG}(k)=\tfrac{1}{2}\sin\phi(k)g(k),$$

$$\mathrm{CG}(k)=\tfrac{1}{2}\cos\phi(k)g(k),$$

$$\mathrm{SP}(k)=k^3\left(\frac{\sin\phi(k)}{k}\right)',$$

$$\mathrm{CP}(k)=k^3\left(\frac{\cos\phi(k)}{k}\right)',$$

$$\mathrm{AA}(k)=k^5\left(\frac{\sin\phi(k)}{k}\right)'',$$

$$\mathrm{CC}(k)=k^5\left(\frac{\cos\phi(k)}{k}\right)'',$$

where the first and the second derivative, with respect to k^2, are denoted by $'$ and $''$, respectively.

REFERENCES

[1] H. Pagels, *Phys. Rep.* **16C**, 219 (1975).

[2] Y. Nambu, G. Jona-Lasinio, *Phys. Rev.* **122**, 345 (1961); **124**, 246 (1961).

[3] M. E. Peskin, *Chiral Symmetry and Chiral Symmetry Breaking*, in *Recent Advances in Field Theory and Statistical Mechanics*. Proceedings of Session XXXIX of the Universite de Grenoble Summer School at Les Houches, J.-B. Zuber and R. Stora, eds. North-Holland, Amsterdam 1984; W. Weise, *Quarks, Chiral Symmetry and Dynamics of Nuclear Constituents*, in *Rev. Nucl. Phys.* **1**, 57 (1985).

[4] E. Dagotto, J. B. Kogut, *Phys. Rev. Lett.* **58**, 299 (1987).

[5] K. D. Lane, *Phys. Rev.* **D10**, 2605 (1974); H. D. Politzer, *Nucl. Phys.* **B117**, 397 (1976); for recent

review see P. I. Fomin, V. A. Miransky, V. P. Gusynin, Y. A. Sitenko, *Riv. Nuovo Cimento* **5**, 1 (1983).

[6] J. Finger, D. Horn, J. E. Mandula, *Phys. Rev.* **D20**, 3253 (1979); J. Finger, J. Weyers, J. E. Mandula, *Phys. Lett.* **96B**, 367 (1980); J. Govaerts, J. E. Mandula, *Nucl. Phys.* **B199**, 168 (1982); J. R. Finger, J. E. Mandula, J. Weyers, *Nucl. Phys.* **B237**, 59 (1984).

[7] A. Amer, A. Le Yaouanc, L. Oliver, O. Pene, J.-C. Raynal, *Phys. Rev. Lett.* **50**, 87 (1983); O. Pene, *Acta Phys. Pol.* **B14**, 499 (1983); A. Le Yaouanc, L. Oliver, O. Pene, J.-C. Raynal, *Phys. Lett.* **134B**, 249 (1984); *Phys. Rev.* **D29**, 1233 (1984); *Phys. Rev.* **D31**, 137 (1985).

[8] A. Casher, *Phys. Lett.* **83B**, 395 (1979).

[9] S. L. Adler, A. C. Davis, *Nucl. Phys.* **B244**, 469 (1984).

[10] V. Shuryak, *Phys. Rep.* **C115**, 151 (1984); J. Kogut et al., *Nucl. Phys.* **B225** [FS9], 93 (1983); P. H. Damgaard, D. Hochberg, N. Kawamoto, *Phys. Lett.* **158B**, 239 (1985); E. M. Ilgenfritz, J. Kripfganz, in Proceedings of the 22nd International Conference on.High Energy Physics, Leipzig 1984, edited by A. Meyer and E. Wieczorek, Akademie der Wissenschaften, Zeuthen, East Germany 1984, p. 57; C. P. van den Doel, *Phys. Lett.* **143B**, 210 (1984).

[11] A. C. Davis, A. M. Matheson, *Nucl. Phys.* **B246**, 203 (1984).

[12] A. Kocic, *Phys. Rev.* **D33**, 1785 (1986).

[13] A. Trzupek, J. Wosiek, *Phys. Rev.* **D33**, 3753 (1986); A. Trzupek, *Acta Phys. Pol.* **B18**, 1141 (1987).

[14] S. L. Adler, T. Piram, *Rev. Mod. Phys.* **56**, 1 (1984).

[15] J. Gasser, H. Leutwyler, *Phys. Rep.* **87C**, 77 (1982).

[16] T. Jaroszewicz, *Acta Phys. Pol.* **B15**, 169 (1984).

[17] T. Barnes, Toronto preprint, UTPT-85-21.

[18] S. L. Adler, *Prog. Theor. Phys.* (Supplement) **86**, 12 (1986).

[19] S. V. Vonsovsky, Yu. A. Izumov, E. Z. Kurmaev, *Superconductivity of Transition Metals*, Springer Series in Solid State Sciences, vol. 27, 1982.

[20] R. Alkofer, P. A. Amundsen, *Phys. Lett.* **B187**, 395 (1987).

[21] A. Trzupek, *Acta Phys. Pol.* **B19**, 179 (1988).

[22] B. Muller, *The Physics of the Quark-Gluon Plasma*, Lecture Notes in Physics, vol. 225, 1985; L. McLerran, *Rev. Mod. Phys.* **58**, 1021 (1986).

[23] L. S. Celenza, A. Rosenthal, C. M. Shakin, *Phys. Rev. Lett.* **53**, 89 (1984); Peng Huang-an, Chao Wei-qing, Liu Lian-sou, Liu Feng, Hua-Zong, preprint, HZPP-84-8.

[24] S. Dubnicka, V. A. Meshcheryakov, J. Milko, *J. Phys. G* **7**, 605 (1981).

[25] C. H. Llewellyn Smith, *Ann. Phys.* (NY) **53**, 521 (1969).

[26] E. Eichten, K. Gottfried, T. Kinoshita, K. D. Lane, T. M. Yan, *Phys. Rev.* **D21**, 203 (1980).

[27] F. Karsch, *QCD at Finite Temperature and Baryon Number Density*, Illinois preprint, ILL-(TH)-85#75, January 1986.